Applied Clay Science 231 (2023) 106745

Contents lists available at ScienceDirect

Applied Clay Science

journal homepage: www.elsevier.com/locate/clay

Research Paper

Adsorption of Pb^{2+} and methylene blue by Al-incorporated magadiite

Qi Sun [a,b,c], Xingqiang Guo [d], Bingchen Guo [c], Qinyuan Tang [c], Wenbin Yu [a,b,*], Quan Wan [a,b,e], Yan An [c,**]

[a] State Key Laboratory of Ore Deposit Geochemistry, Institute of Geochemistry Chinese Academy of Science, Guiyang, Guizhou 550081, China
[b] University of Chinese Academy of Science, Beijing 100049, China
[c] School of Chemistry and Chemical Engineering, Guizhou University, Guiyang, Guizhou 550025, China
[d] School of Resources and Environmental Engineering, Guizhou University, Guiyang, Guizhou 550025, China
[e] CAS Center for Excellence in Comparative Planetology, Hefei, Anhui Province 230026, PR China

ARTICLE INFO

Keywords:
Magadiite
Al-incorporation
Simultaneous adsorption
Cationic dye
Heavy metal
Mechanism

ABSTRACT

The coexistence of heavy metals and organics in industrial wastewater is prevalent, and the removal of these toxic pollutants concurrently is of one of the greatest concerns facing wastewater treatment. In this study, a series of Al-incorporated magadiite (AlMag*x*, *x* represents nominal Si/Al ratio) were synthesized hydrothermally and investigated for their removal of Pb^{2+} and methylene blue (MB) in single- and binary-component solutions. The AlMag*x* featured a higher density of surface hydroxyl groups (6.4–12.7 sites·nm^{-2}) and a greater negative surface than did the Al-free Magadiite (Mag). For single-component adsorption, the adsorption of both pollutants was pH-dependent. Under an optimal pH (= 3.00), the adsorption isotherms for Pb^{2+} and MB were consistent with the Langmuir and Freundlich models, respectively. AlMag240, having the highest surface hydroxyl density, displayed a maximum adsorption capacity of 113.5 and 220.2 mg·g^{-1} for Pb^{2+} and MB, respectively, exceeding that of Mag or other clay minerals. For Pb^{2+}–MB binary-component adsorption, the removal efficiencies of Pb^{2+} declined by ~4%–34% with higher MB concentrations, while MB's adsorption was slightly promoted by co-occurring Pb^{2+}. Examination of adsorption mechanisms revealed that MB was adsorbed onto the external surface of AlMag*x* mainly via hydrogen bonding and electrostatic attraction, while Pb^{2+} was removed by ion exchange and subsequent hydroxyl-facilitated precipitation. The declined adsorption of Pb^{2+} was due to the rapid occupation of negative sites and hydroxyl sites by MB, and the slight promotion of MB adsorption with coexisting Pb^{2+} is likely owing to the increased negative charge of the adsorbents due to the increase in the solution ionic strength. These results demonstrated that the solution component is crucial to the adsorption process and that the AlMag*x* was a new adsorbent for the simultaneous removal of Pb^{2+} and MB.

1. Introduction

Wastewater originating from various industrial activities often contains hazardous inorganic and organic contaminants. Heavy metal ions are the major group of inorganic pollutants in wastewater generated by printing, dyeing, and mining (Uddin, 2017; Georgouvelas et al., 2021). Synthetic dyes, on the other hand, are an important group of organic contaminants, which has been extensively used in textile and leather manufacturing and paper printing (Ngulube et al., 2017; Abdellah et al., 2020; Madduri et al., 2020; Nimbalkar and Bhat, 2021). When discharged into water bodies, either heavy metal ions or synthetic dyes can accumulate and increase the mutagenic and carcinogenic risk to humans and aquatic organisms (Ngulube et al., 2017; Uddin, 2017). Exacerbating the problem, wastewater containing mixed heavy metal ions and organic dyes can be generated by textile, paper, and many other industries (Ajiboye et al., 2021; Bi et al., 2021; Nimbalkar and Bhat, 2021). For example, methylene blue (MB) and Pb^{2+} are widely used as a colorant and mordant in the dyeing process, and the resulting wastewater inevitably contains coexisting toxic pollutants (Chen et al., 2019; Madduri et al., 2020). What is not consistent with the fact that these pollutants usually exist together in environmental and industrial wastewater, most attention has been focused on the individual removal

* Corresponding author at: State Key Laboratory of Ore Deposit Geochemistry, Institute of Geochemistry Chinese Academy of Science, Guiyang, Guizhou 550081, China.
** Corresponding author.
E-mail addresses: yuwenbin@mail.gyig.ac.cn (W. Yu), ruian6901@163.com (Y. An).

https://doi.org/10.1016/j.clay.2022.106745
Received 8 August 2022; Received in revised form 24 October 2022; Accepted 26 October 2022
Available online 4 November 2022

of heavy metals or organic pollutants.

Recently, a few works studied the simultaneous removal of heavy metals or organic pollutants and found they were complex due to either synergistic or antagonistic properties of these pollutions (Ajiboye et al., 2021; Du et al., 2022). Various methods, such as adsorption, ion exchange, photocatalysis, and coagulation are developed for the elimination of coexisting contaminants from wastewater, among which adsorption is quite attractive due to its notable advantages of simplicity, economic feasibility, and efficiency (Abdelhamid, 2020; Kassem et al., 2020; Ajiboye et al., 2021; Bi et al., 2021). Ordered mesoporous carbon, carbon nanotube, graphene oxide composites, and modified clay minerals (such as the montmorillonite-iron system) have been utilized for the removal of heavy metal ions and organic pollutants concurrently from simulated wastewater (Ma et al., 2016; Ma et al., 2018; Madduri et al., 2020; Gang et al., 2021). However, the preparation process of these adsorbents is usually cumbersome, and their removal efficiency depends largely on the chemistry of the metal ions and organics in the solution. Therefore, it is an urgent need for wastewater treatment to synthesize alternative adsorbents with a simple method and study their simultaneous removal performance for multiple pollutants.

Magadiite ($Na_2Si_{14}O_{29}{\cdot}nH_2O$), a kind of hydrated layered polysilicate, is composed of negatively charged silicate layers of SiO_4 tetrahedra and neutralizing Na^+ in the interlayer space (dos Santos et al., 2022). Magadiite has several attractive physicochemical properties, such as high cation exchange capacity (2.0 meq/g), reactive silanol groups, and interlayer swelling, rendering it garnering extensive attention in environmental remediation (Ide et al., 2011; Ding et al., 2018; França et al., 2019). In previous research, it was reported that magadiite could efficiently remove cationic organic contaminants (e.g. methylene blue, phenol, and ranitidine) or heavy metal ions (Cu^{2+}, Zn^{2+}, Cd^{2+}, Pb^{2+}, and In^{3+}) from water (Homhuan et al., 2017; Ding et al., 2018; Ge et al., 2018; França et al., 2019; Mokhtar et al., 2020; Sruamsiri et al., 2021), but the adsorption capacity was limited by its cation exchange capacity.

Heteroatoms such as aluminum can be easily introduced into the silicate framework of magadiite (Moura et al., 2011; Bi et al., 2012; Oliveira et al., 2015). By incorporation of aluminum, on one hand, the permanent negative charge of magadiite can be augmented due to the isomorphic substitution of silicon atoms by lower valence aluminum atoms (Almeida et al., 2019), and on the other hand, more hydroxyl groups could be introduced in the sample due to localized defects formed (Superti et al., 2007). Given that negative sites and hydroxyl groups are both key adsorption sites for capturing pollutants (Ide et al., 2011; Lim et al., 2017; França et al., 2019), the Al-incorporated magadiite is expected to outperform its preceding silicic counterpart in adsorption performance. However, so far, little effort has been expended towards investigating the adsorption performance of Al-incorporated magadiite, let alone the simultaneous adsorption of organic and inorganic contaminants, so the effect of the Al-incorporation process on the adsorption performance of magadiite remains an open question.

In the present study, a series of Al-incorporated magadiite (AlMag*x*) were synthesized hydrothermally and investigated for the removal of heavy metal and organic pollution individually and simultaneously. Pb^{2+} and MB were selected as model heavy metal and organic pollutants, respectively, and the influences of wastewater components on the adsorption performance of AlMag*x* were focused on. The synthetic adsorbents were systematically characterized to determine the influence of Al-incorporation on the microstructure and surface properties. The adsorption performance of the AlMag*x* was first investigated for single-component Pb^{2+} or MB adsorption, by the batch method, and this was then extended to Pb^{2+}–MB binary-component adsorption. The adsorbents recovered from the above adsorption experiments were further analyzed to explore the interaction mechanisms between multiple pollutants and the adsorbents.

2. Materials and methods

2.1. Materials, preparation and characterization of samples

The materials, synthesis, and characterization of the Al-incorporated magadiite (denoted as AlMag*x*, *x* refers to nominal Si/Al ratio), as well as siliceous magadiite (Mag), are shown in the Supplementary Information (SI).

2.2. Adsorption experiments in single-component solutions

The removal of Pb^{2+} or MB from their corresponding single-component solutions was carried out using the batch method. These adsorption experiments were conducted in triplicate, each in a reciprocating shaker at 25.0 ± 0.5 °C.

The effect of initial pH was investigated by mixing 50 mg of adsorbent with 50 mL of solution. The initial concentration of Pb^{2+} or MB was set at 100 mg·L^{-1}. Initial pH values of the Pb^{2+} and MB solutions were respectively adjusted to range from 2.00 to 5.00 and from 2.00 to 10.00, by adding 0.1 mol·L^{-1} HCl or NaOH as needed. The initial pH of single Pb^{2+} solutions was kept below 6.00 to avoid possible precipitation (Madduri et al., 2020). Each prepared mixture was shaken for 360 min, to achieve equilibrium before its analysis. Adsorption kinetic experiments were performed by mixing 500 mg of adsorbents with 500 mL of solution at optimal initial pH (3.00 ± 0.05). The initial concentration of Pb^{2+} or MB was 100 mg·L^{-1}. Adsorption isotherms were obtained at initial concentrations that spanned 5 to 600 mg·L^{-1} for either adsorbate. Based on the preliminary experiment's results, the solution pH and contact time were set at 3.00 ± 0.05 and 360 min, respectively. After completing the adsorption experiments, the adsorbents were recovered by centrifugation, and the supernatant was collected for further analysis.

The final Pb^{2+} concentration was determined by atomic absorption spectrometry (Thermo Scientific iCE 3500), while the MB concentration was analyzed through UV–Vis spectrophotometry (Mapada UV6100S) at its maximum absorbance of 665 nm. The removal efficiency (Efficiency, %) and adsorption capacity (q_t, mg·g^{-1}) of adsorbates were calculated according to Eqs. 1 and 2, respectively.

$$\text{Efficiency} = \frac{C_0 - C_t}{C_0} \times 100 \tag{1}$$

$$q_t = \frac{(C_0 - C_t)}{m} V \tag{2}$$

where C_0 and C_t (mg·L^{-1}) are respectively the initial and residual concentrations after adsorption for the contact time *t* of the adsorbate, with *m* (g) and *V* (L) denoting the weight of the adsorbent and volume of the solution, respectively.

2.3. Adsorption experiments in binary-component solutions

Adsorption experiments in binary-component solutions were conducted to investigate the simultaneous removal of Pb^{2+} and MB. To examine the influence of co-occurring MB upon the adsorption of Pb^{2+}, the initial concentration of Pb^{2+} was fixed at 100 mg·L^{-1} with the MB concentration ranging from 25 to 100 mg·L^{-1}. Conversely, the MB concentration was held at 100 mg·L^{-1} with Pb^{2+} concentration spanning from 25 to 100 mg·L^{-1} to study the effect of co-occurring Pb^{2+} upon MB's removal. Based on the results of single-component experiments, the initial pH of all tested binary systems was adjusted to 3.00 ± 0.05, with a twofold contact time (720 min) used to ensure an adsorption equilibrium was attained. The Pb^{2+} and MB concentrations were analyzed in the same manner as described above for the single-component experiments. Finally, the mutual effects between MB and Pb^{2+} were determined by comparing the removal efficiencies in binary systems with those obtained in single-component systems under similar experimental conditions.

2.4. Recyclability

The recyclability of the adsorbents was studied through repeated adsorption-desorption processes in the single-component system. The recovered adsorbents were repeatedly washed with 0.1 mol·L^{-1} HCl and 1% HCl/ethanol (*v*/v) to unload the adsorbed Pb^{2+} and MB, respectively. After thorough desorption, the samples were regenerated by 0.05 mol·L^{-1} NaOH before being subjected to the next run.

3. Results and discussion

3.1. Characterization of the adsorbents

Mag and AlMag*x* (Fig. 1A) show characteristic XRD patterns similar to those previously reported (Superti et al., 2007; Bi et al., 2012), albeit a trace amount of mordenite impurities appears in AlMag120 (Fig. 1A (d)). The strong peak at 5.7° (2θ), and two weak ones at 11.4° and 17.1°correspond to (001), (002), and (003) reflections, respectively. The basal spacing of the AlMag*x* samples is identical to that of Mag (1.56 nm), suggesting aluminum's presence does not alter the interplanar distance. A group of well-defined peaks between 22° and 30° indicates the crystalline nature of the silicate lamellas even after modification with different amounts of aluminum (Superti et al., 2007). The ^{27}Al MAS NMR spectra of three AlMag*x* samples show a predominant signal at 57 ppm (Fig. 1B), indicating Al mainly presented as tetrahedral coordination in the samples (Zebib et al., 2006). A weak but broad band around 0 ppm appears only in AlMag120 (Fig. 1B(d)), attributable to the extra-framework Al in octahedral coordination (Moura et al., 2011; Bi et al., 2012).

As shown by SEM (Fig. S1) and TEM (Fig. S2) images, Mag and AlMag*x* all display the typical rosette-like morphology originating from the intergrowth of well-crystallized silicate sheets. Yet the silicate layers of AlMag*x* became smaller with more Al included (Fig. S1b–d), which could be explained by a decreased crystallization rate in the presence of aluminum (Bi et al., 2012). The Si/Al molar ratio based on EDS results (Si/Al_{exp}) is slightly lower in final solids than the starting gel (Table 1), likely due to the higher solubility of the silicon species than aluminum species in the synthesis liquor (Almeida et al., 2019). The FT-IR spectra of AlMag*x* samples present enhanced OH stretching bands in the 3200–4000 cm^{-1} region compared with Mag, due to the increased number of hydroxyl groups upon Al incorporation, while the stretching and bending vibrations of Si-O-Si in the 400–1400 cm^{-1} region are not significantly altered (Fig. S3). The N_2 adsorption-desorption isotherms of Mag and AlMag*x* adsorbents (Fig. S4) can be assigned to IV(a) type with H3-type hysteresis loop according to the updated IUPAC classification (Thommes et al., 2015). The BET surface area (S_{BET}) and pore volume (V_p) of all AlMag*x* samples are smaller than those of Mag (Table 1), possibly due to the contact packing of lamellas upon Al incorporation. S_{BET} and V_p of AlMag480 and AlMag240 tend to gradually diminish with an increasing Al content, while AlMag120 exhibited relative larger S_{BET} and V_p, probably attributing to the existence of microporous mordenite in this sample (Fig. 1d).

Table 1
Structural parameters of Mag and the three AlMag*x* samples having a different Si/Al ratio.

Samples	Si/Al_{exp} [a]	S_{BET} ($m^2 \cdot g^{-1}$) [b]	V_p ($cm^3 \cdot g^{-1}$)	D_s (sites·nm^{-2})
Mag	∞	32.09	0.12	4.7
AlMag480	420	25.62	0.11	6.4
AlMag240	211	19.37	0.07	12.7
AlMag120	112	25.32	0.10	8.7

[a] Based on the EDS results.
[b] Calculated from the N_2 adsorption isotherm.

As shown in Fig. 2, the isoelectric point of Mag is 2.30, while all AlMag*x* samples are constantly negatively charged in the pH range of 2.00–10.00. Moreover, sample with a higher Al content tends to exhibit a more negative surface. These results can be explained by the fact that the replacement of Si by Al in the magadiite layers created more negatively charged sites in the samples. The density of surface hydroxyl groups (denoted as D_S) was measured and the results were listed in Table 1. The D_S of AlMag*x* was 6.4–12.7 sites·nm^{-2} (Table 1), these being 1.4–2.7 times higher than that of Mag (4.7 sites·nm^{-2}). Notably, AlMag240 has the highest D_s among all tested AlMag*x* samples. The significantly increased D_S can be ascribed to localized defects that

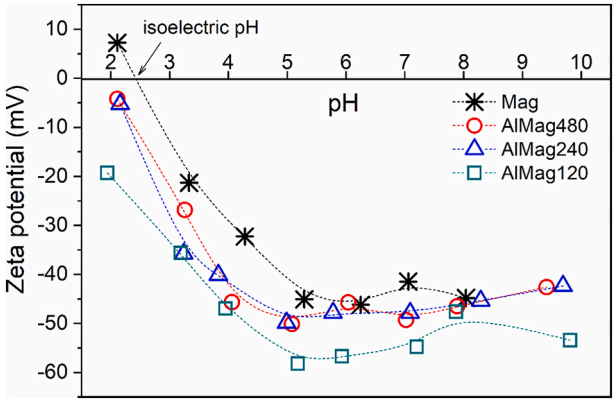

Fig. 2. Zeta potentials of Mag and AlMag*x*.

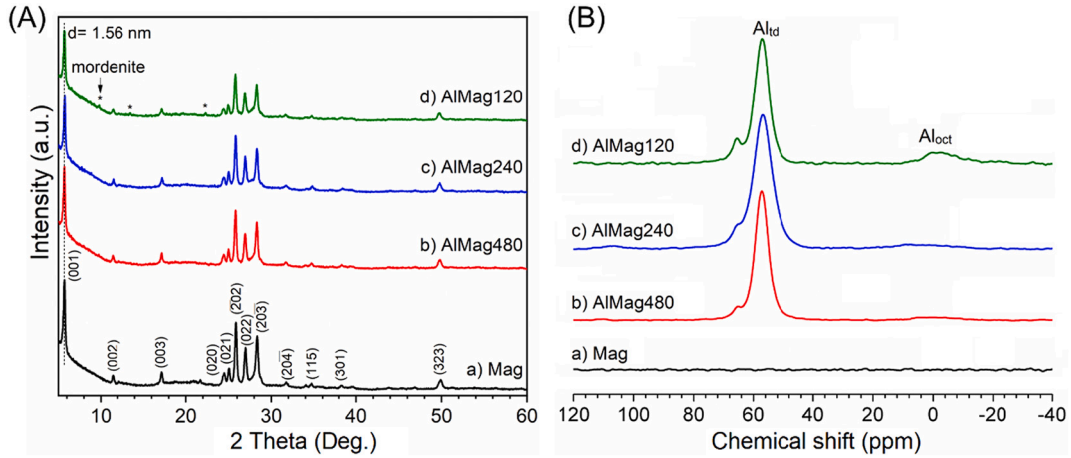

Fig. 1. XRD patterns (A) and ^{27}Al MAS NMR spectra (B) of Mag (a) and three AlMag*x* samples with different Si/Al ratios (b–d).

expose more surface hydroxyl groups as a result of Al incorporation (Superti et al., 2007; Moura et al., 2011).

3.2. Adsorption performance of the adsorbents

3.2.1. Effect of solution pH

pH is a critical factor that influences the adsorption process because pH can affect both the speciation of adsorbate and the surface charge of the adsorbent. The removal efficiency as a function of the initial solution pH is depicted in Fig. 3. In the case of Pb^{2+} (Fig. 3A), all adsorbents have rather low removal efficiencies when the pH is 2.00, but they increase abruptly at pH 3.00, and then continued to slightly increase with rising pH levels. Previous reports reveal that the adsorption of metallic cations by magadiite is primarily an ion-exchange-controlled process, in which electrostatic interaction is the dominant interaction force (Murakami et al., 2006; Ide et al., 2011; Homhuan et al., 2017). It is worth pointing out that those reported adsorption experiments were conducted under neutral conditions. In acidic solutions, the interference of coexisting H^+ should be considered, given the high affinity of protons to the silicate surface (Murakami et al., 2006). At pH 2.00, the H^+ concentration was 10 mmol·L^{-1}, >20 times higher than the Pb^{2+} concentration (100 ppm, 0.48 mmol·L^{-1}). Therefore, the interlayer Na^+ of the adsorbents (ca. 1.8 mmol·g^{-1}, based on the calculated molecular formula (Sun et al., 2014)) would preferentially exchange with H^+ to form H-magadiite, resulting in the non-removal of Pb^{2+}. When the H^+ concentration decreased to 1.0–0.01 mmol·L^{-1} (pH 3.00–5.00), Pb^{2+} would compete with H^+ in the ion exchange process, leading to significantly increased removal efficiencies. Over the investigated pH range, all three AlMag*x* adsorbents exhibited higher removal efficiencies than Mag. This is because AlMag*x* is more negatively charged than Mag, which increases the ion exchange capacity of Pb^{2+} into the interlayer. Moreover, it is reported that hydroxyl groups could further react with the interlayer Pb^{2+} to form hydroxide nanoparticles that precipitate onto the surface of magadiite (Lim et al., 2017) (Fig. S5). The high density of surface hydroxyl sites and the basic nature of newly-formed aluminols (Tombácz and Szekeres, 2004) on AlMag*x* would possibly promote this precipitation reaction. Consequently, AlMag*x* exhibited higher adsorption efficiencies than Mag. Among all adsorbents, AlMag240 has the greatest Pb^{2+} removal rate at the initial pH of 5.00.

In the case of MB (Fig. 3B), the varied removal efficiency associated with pH level indicates that multiple interactions may be involved in the adsorption process based on the speciation of MB (Madduri et al., 2020). At pH 2.00, non-charged MB is the predominant species in aqueous solutions (Fig. S6), and hydrogen bonding would be the major interaction between nitrogen atoms of neutral MB molecules and surface hydroxyl groups of the adsorbents (Al-Ghouti et al., 2010; França et al., 2019). At pH 3.00, we found that 86% of MB existed in its neutral form and 14% in its cationic form (Fig. S6). In addition to hydrogen bonding, positively charged MB dye may be adsorbed on the negative external surfaces or edges of adsorbents via electrostatic attraction. Besides, intermolecular interactions between the adsorbed MB and free MB molecules may also happen through hydrogen bonding or the π–π stacking of aromatic rings (Ovchinnikov et al., 2016). All these factors contributed to a high removal efficiency at pH 3.00. When the solution pH increased to 4.00 and higher, MB existed primarily in the cationic form (Fig. S6); thus, ion exchange would be the predominant interaction under these conditions (see Section 3.3). The removal efficiency is reduced due to the rejection between the adsorbed and free cationic MB, as well as the slightly increased zeta potentials of the adsorbents (Fig. 2). Considering AlMag*x* samples have a higher density of surface hydroxyl sites and a more negative surface than Mag, they hence exhibit a higher ability to interact with neutral and cationic MB molecules via hydrogen bonding and electrostatic interaction, respectively. Among the three AlMag*x* adsorbents, AlMag240 is able to completely remove MB at pH 3.00, possibly due to it having the highest density of surface hydroxyl sites. It should be noted that the trends of MB removal by AlMag*x* as a function of pH differed markedly from other synthetic magadiites in previous reports (Royer et al., 2009; Mokhtar, 2017), a discrepancy which can be ascribed to different surface charges of these adsorbents at an identical pH level. In our cases, the surface charge of AlMag*x* stays negative over the pH range of 2.00–10.00 whereas magadiite reportedly only becomes negative at pH > 4.50 (Royer et al., 2009) or 5.10 (Mokhtar, 2017). Based on the removal efficiencies of Pb^{2+} and MB, subsequent experiments were done at the optimal pH of 3.00 for the initial solution.

3.2.2. Effect of contact time

The effect of contact time on the adsorption of Pb^{2+} and MB by the prepared adsorbents is shown in Fig. 4. For all three AlMag*x* adsorbents, the adsorption process was very fast in the initial 30 min, and then gradually attained equilibrium after 360 and 240 min for Pb^{2+} and MB, respectively. Note that a faster equilibrium of MB was achieved than Pb^{2+} in all cases, implying the different interactions between AlMag*x* and the two tested pollutants. The adsorption capacities of AlMag*x* for Pb^{2+} were 64.6–87.9 and 85.3–94.1 mg·g^{-1} at 30 min and equilibrium, respectively, while those for MB were 79.9–92.1 and 89.0–98.6 mg·g^{-1} at the same time interval. Over 75% and 90% of total adsorbed Pb^{2+} and MB, respectively, were removed in the first 30 min, which might be an advantage of AlMag*x* samples as novel adsorbents. By contrast, Mag exhibited much slow adsorption for both pollutants, and only 42% and 70% of total Pb^{2+} and MB, respectively, were removed in the initial 30 min. The equilibrium adsorption capacities of Mag were 83.5 mg·g^{-1} for Pb^{2+} and 81.8 mg·g^{-1} for MB, both of which were smaller than those of AlMag*x*. These results indicated that Al incorporation substantially

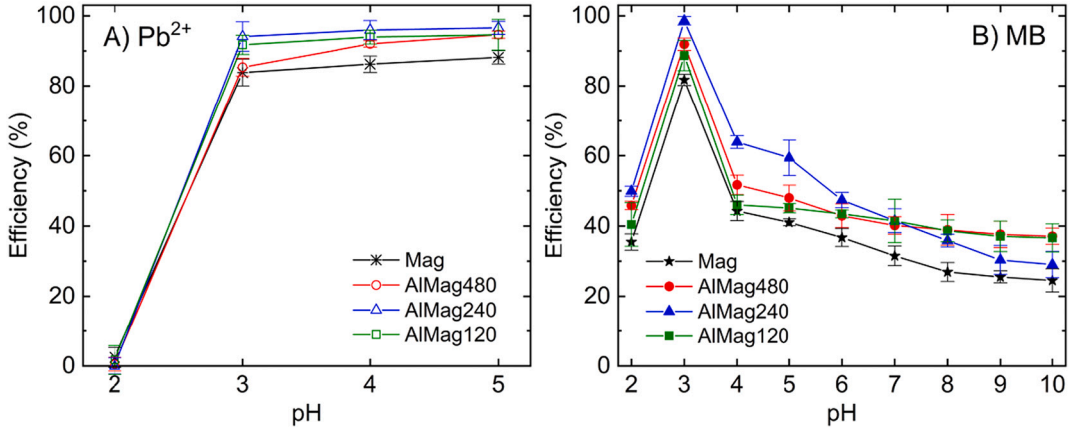

Fig. 3. Effect of pH on the adsorption of Pb^{2+} (A) and MB (B) by Mag and the AlMag*x* samples.

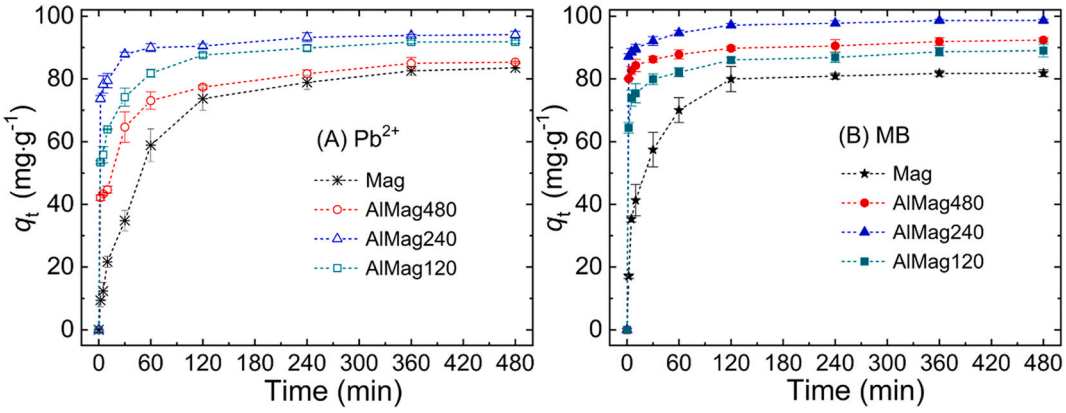

Fig. 4. Effect of contact time on the adsorption of Pb^{2+} (A) and MB (B) by Mag and the AlMag*x* samples.

increased the adsorption rates as well as adsorption capacities of AlMag*x* samples.

3.2.3. *Effect of initial concentrations*

The equilibrium adsorption capacities (q_e) of both pollutants at different initial concentrations are depicted in Fig. S7. The $q_{e,MB}$ values continue to increase when the initial concentration rises from 10 mg·L^{-1} to 600 mg·L^{-1}, whereas the $q_{e,Pb}$ values remain nearly constant at an initial concentration > 200 mg·L^{-1}. To provide insight into how either adsorbate interacted with the as-synthesized adsorbents, Langmuir (Eq. 3) and Freundlich (Eq. 4) isotherm models were each fitted to the experimental data (Ngulube et al., 2017; Al-Ghouti and Da'ana, 2020).

$$q_e = \frac{q_m K_L C_e}{1 + K_L C_e} \tag{3}$$

$$q_e = K_F C_e^{1/n_F} \tag{4}$$

where q_e (mg·g^{-1}) and C_e (mg·L^{-1}) are the adsorption capacities and concentrations of the adsorbate at equilibrium; q_m (mg·g^{-1}), K_L (L·mg^{-1})/K_F (mg·g^{-1}), and n_F respectively denote the maximum adsorption capacity of a given adsorbate, the energy constant, and the adsorption intensity.

According to the R^2-values obtained and the consistency between the

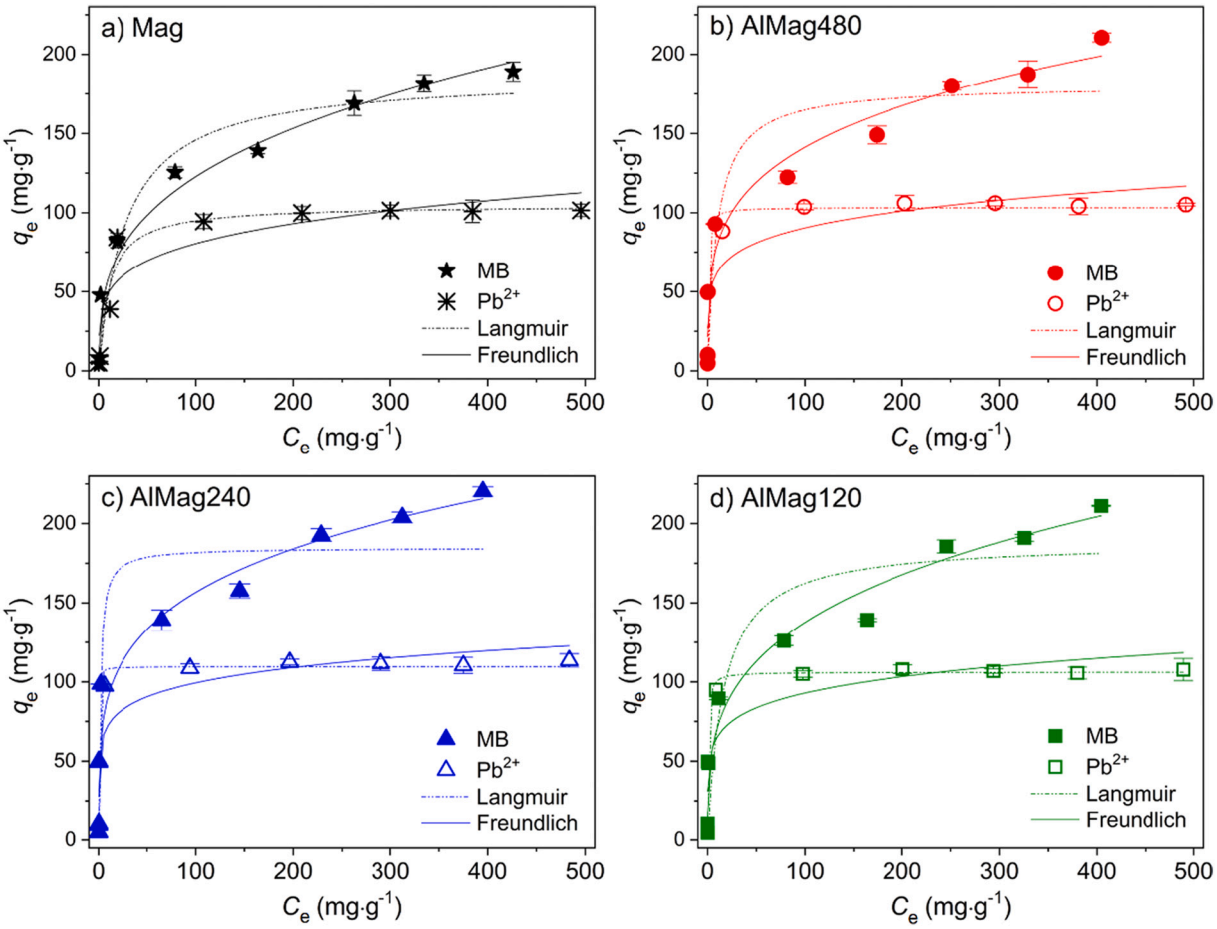

Fig. 5. Adsorption isotherms of Pb^{2+} and MB for the Mag (a) and the three AlMag*x* (b–d) adsorbents.

experimental and calculated q_m values (Fig. 5, Table 2), the Langmuir model better describes the Pb^{2+} adsorption isotherms. This finding is consistent with previous reports on the ion exchange of magadiite with other metal ions (Homhuan et al., 2017; Lim et al., 2017). For MB, the adsorption isotherms are better fitted with the Freundlich model, indicating that its adsorption possibly occurs in a multi-layer manner (Al-Ghouti and Da'ana, 2020). In fact, the speciation of MB strongly influences the shape of its adsorption isotherm: that in basic solution is better fitted by the Langmuir model (Fig. S8). Even though the fitted isotherms are insufficient to directly reflect the adsorption mechanisms, the fitted results clearly indicate that Pb^{2+} and MB interact differently with AlMag*x* in acidic solutions.

AlMag*x* samples had higher adsorption capacity ($q_{m,\ exp}$) for both Pb^{2+} and MB than did Mag. For example, the $q_{m,exp}$ values of AlMag240 for Pb^{2+} and MB are 113.5 and 220.2 $mg{\cdot}g^{-1}$ (Table 2), which are ~12% and 16% higher than those of Mag, respectively. If evaluated by the surface area (Fig. S9), the adsorption capacities of AlMag240 (Pb^{2+} 5.9 $mg{\cdot}m^{-2}$, MB 11.4 $mg{\cdot}m^{-2}$) would be approximately twice those of Mag. These results emphasize the essential role of Al-incorporation in increasing the adsorption capacity of magadiite. Moreover, the AlMag*x* adsorbents can effectively remove Pb^{2+} and MB from acidic solutions, thus outperforming other reported clay minerals under similar adsorption conditions (Table S1). This, combined with its easy synthesis, fast adsorption rate, and high adsorption capacities, suggest AlMag*x* harbors potential as a superior adsorbent, one apt for the treatment of acidic wastewater.

3.2.4. Simultaneous adsorption of Pb^{2+} and MB

To study the simultaneous adsorption performance of Mag and the three AlMag*x*, we conducted adsorption experiments using the Pb^{2+}–MB binary-component, at pH 3.00, and compared their removal efficiencies with those from the single-component experiments. The complexation of Pb^{2+} with MB, which may lead to species being more prone to adsorption, is precluded here because this reaction is strongly inhibited in acidic environments (Ghaedi et al., 2015). The precipitation of Pb^{2+} is precluded by the fact that the final-solution pH values of all binary solutions (Table S2) were always lower than the calculated pH from K_{sp} of $Pb(OH)_2$ amounting to 1.43×10^{-20} (Liu and Liu, 2003). When the initial concentration of Pb^{2+} was fixed at 100 ppm, the removal efficiency of Pb^{2+} gradually decreased as the MB concentration increased (Fig. 6A). The removal efficiency of Pb^{2+} was ~4% to 34% lower in the binary-component adsorption than single-component adsorption. For instance, the removal efficiency of Pb^{2+} by AlMag240 was as high as 94% in the single-component adsorption but this declined to 81%–63% with more MB present in the binary-component adsorption. By contrast, the stepwise increment of the Pb^{2+} concentration promoted the MB's adsorption (Fig. 6B). During binary-component adsorption, the AlMag*x* adsorbents showed slightly enhanced MB removal efficiencies in the binary solutions, achieving nearly complete removal of MB when co-occurring Pb^{2+} concentration reached 100 ppm. These results also indicated that the selectivity towards MB was higher than Pb^{2+} for all adsorbents. In all binary-component systems, AlMag*x* samples show higher removal efficiency for Pb^{2+} and MB than Mag, benefitting from the more negative surface and higher surface site density upon Al-incorporation.

The mutual effect of coexisting Pb^{2+} and MB for their simultaneous adsorption on all adsorbents can be gauged by the ratio of adsorption capacity ($R_{q,i}$, Equation5):

$$R_{q,i} = \frac{q_{b,i}}{q_{s,i}} \tag{5}$$

where $q_{b,i}$ and $q_{s,i}$ are the adsorption capacity of pollutant *i* in the binary- and single-component system with the same initial concentration, respectively. According to previous reports (Zhao et al., 2015; Chen et al., 2019), three cases are possible under simultaneous adsorption: (i) If $R_{q,i} > 1$, the adsorption of pollutant *i* is enhanced by the presence of the co-pollutant. (ii) If $R_{q,i} < 1$, the adsorption of pollutant *i* is suppressed by the presence of the co-pollutant. (iii) If $R_{q,i} = 1$, the adsorption of pollutant *i* is negligibly influenced by the presence of the co-pollutant. The $R_{q,i}$ values are plotted as a function of the co-pollutant's concentration. The trend for $R_{q,Pb}$ (Fig. 6C) is of monotonic decline with increasing MB concentration, implying the adsorption of Pb^{2+} is intimately influenced by co-occurring MB. However, $R_{q,MB}$ (Fig. 6D) increases slightly along with increasing Pb^{2+} concentration, which suggests the uptake of MB is promoted by co-occurring Pb^{2+}. The coexisting adsorption inhibition and promotion can be ascribed to the different adsorption mechanisms for Pb^{2+} and MB by the adsorbents.

The recyclability of AlMag*x* samples was studied through repeated adsorption-desorption processes in single-component solutions. The adsorption efficiency of Pb^{2+} (Fig. S10A) slightly declined in the first cycle and remained >80% in the following 2 cycles, and the MB adsorption efficiency (Fig. S10B) also remained >80% of those of the fresh adsorbents after the third cycle. All these results suggested the stability and reusability of AlMag*x* adsorbents in potential practical applications.

3.3. Adsorption mechanism

To further elucidate the possible interaction between the adsorbents and adsorbates, all samples were recovered after the adsorption

Table 2
Isotherm parameters of Langmuir and Freundlich models for Pb^{2+} and MB adsorption[a].

Pollutant	Sample	$q_{m,exp}$ ($mg{\cdot}g^{-1}$)	Langmuir			Freundlich		
			q_m ($mg{\cdot}g^{-1}$)	K_L ($L{\cdot}mg^{-1}$)	R^2	K_F ($mg{\cdot}g^{-1}$)	n_F	R^2
Pb^{2+}	Mag	101.5	104.9 (4.7)	0.09 (0.02)	0.9539	30.55 (8.39)	4.76 (0.21)	0.8522
	AlMag480	105.1	103.3 (2.4)	1.83 (0.36)	0.9810	43.13 (8.48)	6.23 (0.34)	0.8500
	AlMag240	113.5	109.5 (2.0)	8.13 (1.35)	0.9881	53.63 (9.03)	7.47 (0.35)	0.8460
	AlMag120	107.6	106.1 (2.2)	1.93 (0.34)	0.9848	46.01 (9.72)	3.51 (0.39)	0.8025
MB	Mag	189.1	186.6 (13.7)	0.04 (0.01)	0.9393	28.01 (5.54)	3.12 (0.36)	0.9654
	AlMag480	210.6	180.8 (15.9)	0.10 (0.07)	0.8601	45.07 (8.52)	4.08 (0.34)	0.9583
	AlMag240	220.2	184.7 (12.5)	0.60 (0.34)	0.8935	53.62 (10.04)	4.30 (0.34)	0.9537
	AlMag120	211.0	188.4 (16.7)	0.06 (0.03)	0.8875	37.07 (6.61)	6.55 (0.32)	0.9696

[a] Initial pH = 3.00 ± 0.05, contact time = 360 min. Data in parenthesis represent the standard errors determined by the fitting.

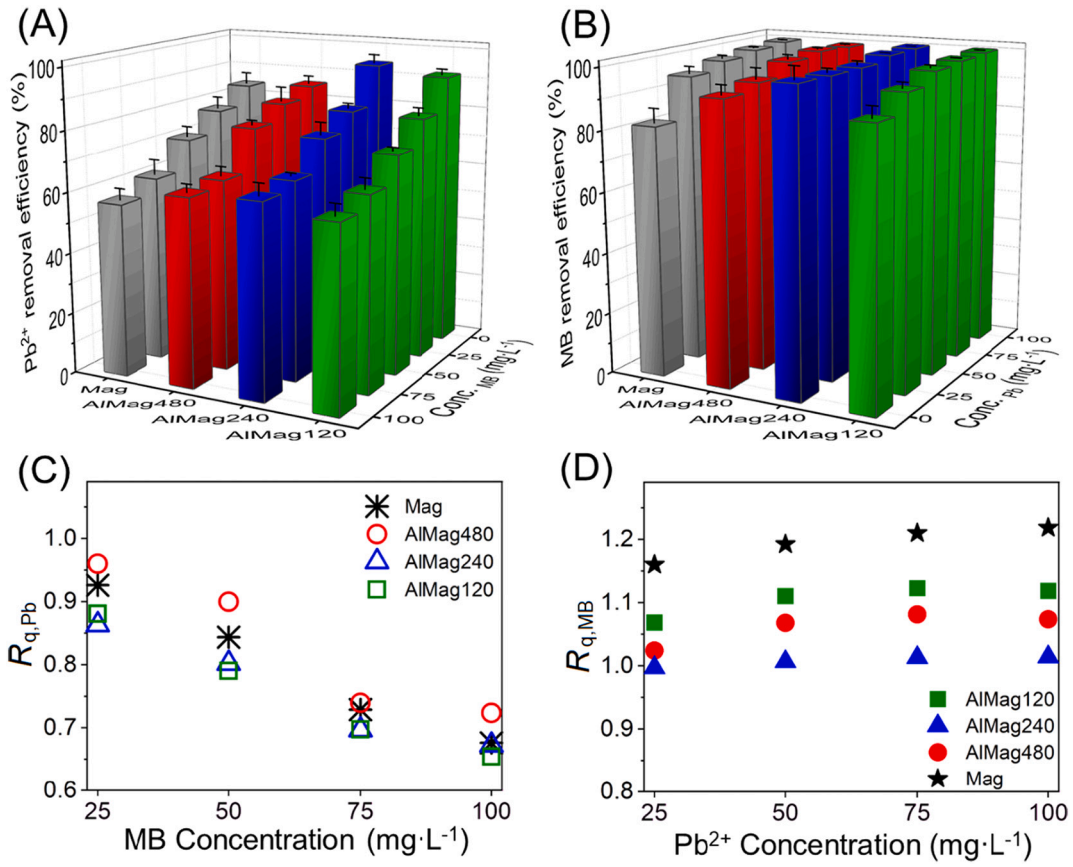

Fig. 6. Removal efficiencies of Pb^{2+} (A) and MB (B) in binary Pb^{2+}–MB solutions by the adsorbents, and the ratio of adsorption capacities ($R_{q,i}$) as a function of the concentration of co-occurring MB (C) or Pb^{2+} (D).

experiments and characterized by XRD. After the single Pb^{2+} adsorption, the $d_{(001)}$ of all AlMag*x* (Fig. 7A) decreased to 1.34 nm from 1.56 nm. The estimated gallery height (GH) of AlMag*x* is 0.22 nm after adsorption (GH = $d_{(001)}$ – 1.12 nm, where 1.12 nm is the thickness of the magadiite layer (Mokhtar et al., 2020)). Given the hydrated and ionic diameters of Pb^{2+} ions are approximately 0.80 nm (Ding et al., 2018) and 0.196 nm (Shannon, 1976), respectively, Pb^{2+} could enter the interlayer space of AlMag*x* by ion exchange in a dehydrated or partially hydrated form (Murakami et al., 2006; Lim et al., 2017). All AlMag*x* adsorbents after their adsorption of MB (Fig. 7B) displayed sharp diffraction lines with a $d_{(001)}$ of 1.42 nm. The decrease of $d_{(001)}$ after adsorption of MB could attribute to the exchange of interlayer Na^+ by H^+ and differences in the hydration degree of the sample. The estimated GH is 0.30 nm, which is smaller than the MB molecule's dimensions (1.34 × 0.60 × 0.38 nm (Zhao et al., 2015)). Therefore, MB molecules could possibly be adsorbed onto the external surfaces or edges of AlMag*x* via hydrogen bonding and electrostatic attraction, respectively. Yet for a solution at pH ≥ 4.00, the estimated GH from the XRD results of recovered adsorbents (Fig. S11) increased to 0.44 nm, which could accommodate MB molecules in a monolayer parallel to the silicate layer, being quite similar to the arrangement of organic ranitidine in the interlayer space of Na-magadiite (França et al., 2019). After adsorption in Pb^{2+}–MB solutions (Fig. 7C), all AlMag*x* had values of 1.38 nm for $d_{(001)}$ and 0.26 nm for GH, which is large enough to accommodate dehydrated Pb^{2+} cations, but still too small for MB molecules to occupy. Hence, we inferred that MB molecules were primarily adsorbed onto the external surface, while Pb^{2+} cations existed in the interlayer space of the AlMag*x* at pH = 3.00.

The morphological changes of the samples after the adsorption

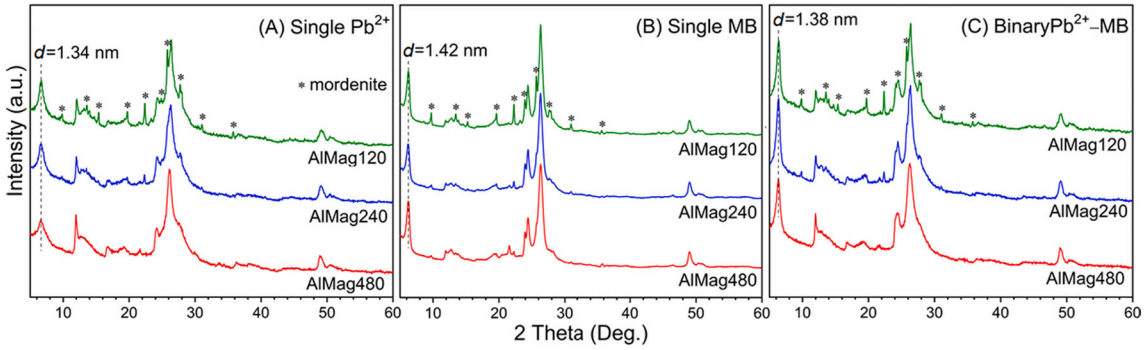

Fig. 7. XRD patterns of AlMag*x* samples after adsorption of Pb^{2+} (A), MB (B), and Pb^{2+}–MB (C). The initial pH of all solutions was adjusted to 3.00. Initial concentrations of MB and/or Pb^{2+} were maintained at 100 ppm in both single- and binary-component solutions.

experiments were studied by SEM and TEM, and the results were displayed in Fig.S12 and Fig. S13. The rosette-like morphology of the samples was maintained after the adsorption experiments in both single- and binary-component solutions (Fig. S12). The appearance of lead nanoparticles on the external surface of Al-magadiite supports the proposed adsorption mechanism involving surface precipitation between adsorbed Pb^{2+} and surface hydroxyl sites of the adsorbents (Fig. S13).

In summary, the simultaneous adsorption of Pb^{2+} and MB by the prepared AlMag*x* adsorbents can be explained by comprehensive joint contribution of ion exchange, surface-precipitation, hydrogen bonding, and electrostatic attraction under the tested conditions (Fig. 8). In the single Pb^{2+} system, Pb^{2+} ions are removed by an ion-exchange reaction with the interlayer Na^{+} of the adsorbents and the exchanged Pb^{2+} could further react with hydroxyl groups to precipitate nanoparticles that are randomly distributed on the adsorbents' external surface (Fig. 8A). For the single MB solution, the small amount of cationic MB in it interacts with the negative surface sites via electrostatic attraction, while the neutral MB molecules are adsorbed onto the external surface of the solid adsorbents through hydrogen bonding with surface hydroxyl groups or through intermolecular interaction (π–π stacking) with the adsorbed MB (Fig. 8B). In the binary Pb^{2+}–MB solution, MB molecules are faster adsorbed by the adsorbents through hydrogen bonding and electrostatic attraction, and the electrostatic attraction of cationic MB is slightly promoted due to increased ionic strength (IS) of the solution when coexisting with Pb^{2+}. This is because the surface charge of clay minerals tended to be more negative with higher IS at a certain pH value (Hao et al., 2018). Nonetheless, Pb^{2+} adsorption efficiencies are sensitive to the concentration of coexisting MB, this attributes to the fast occupation of surface sites by MB that impedes ion exchange and the later hydroxyl-facilitated precipitation of Pb^{2+} (Fig. 8C).

4. Conclusions

This work is the first to report on the simultaneous removal of Pb^{2+} and MB from aqueous solutions by Al-incorporated magadiite (AlMag*x*). Detailed characterizations revealed that most of the Al were incorporated into the silicate framework in tetrahedral form, resulting in a well-kept layered structure, slightly decreased surface area, constantly negative surface over the pH range of 2.00–10.00, and a significantly increased density of surface hydroxyl sites (6.4–12.7 sites·nm^{-2}), when compared with the Al-free Mag. In single-component adsorption experiments, the removal efficiencies of both Pb^{2+} and MB depended strongly on pH. The AlMag*x* adsorbents showed high removal efficiencies for Pb^{2+}(> 85%) and MB (> 95%) at pH 3.00 and an initial concentration of 100 mg·L^{-1}, exceeding those of Mag. The adsorption isotherms of Pb^{2+} and MB by AlMag*x* could be well described by Langmuir and Freundlich model, respectively. AlMag240, with a Si/Al ratio of 240, harbored the highest adsorption capacity of 113.5 mg·g^{-1} for Pb^{2+} and 220.2 mg·g^{-1} for MB, being higher than silicic Mag or other reported clay minerals under similar conditions. In binary Pb^{2+}–MB solutions, MB was preferentially adsorbed onto the external surface of the adsorbents mainly via hydrogen bonding and electrostatic attraction, and the coexisting Pb^{2+} slightly promoted its adsorption due to the increased surface negative charge with increasing solution ionic strength. Yet Pb^{2+} adsorption was proportionally interfered with by MB due to its fast occupation of surface sites hindered ion exchange and subsequent hydroxyl-facilitated precipitation of Pb^{2+}. The AlMag*x* adsorbents can be regenerated and maintained satisfactory removal performance for both pollutants after three adsorption-desorption cycles, suggesting their potential practical applications. Our study manifests the essential role of Al-incorporation in increasing the adsorption capacity of magadiite and the importance of solution components in the adsorption process. This work also demonstrated the potential application of Al-incorporated magadiite as a novel adsorbent for the simultaneous removal of toxic inorganic and organic pollutants from aqueous solutions.

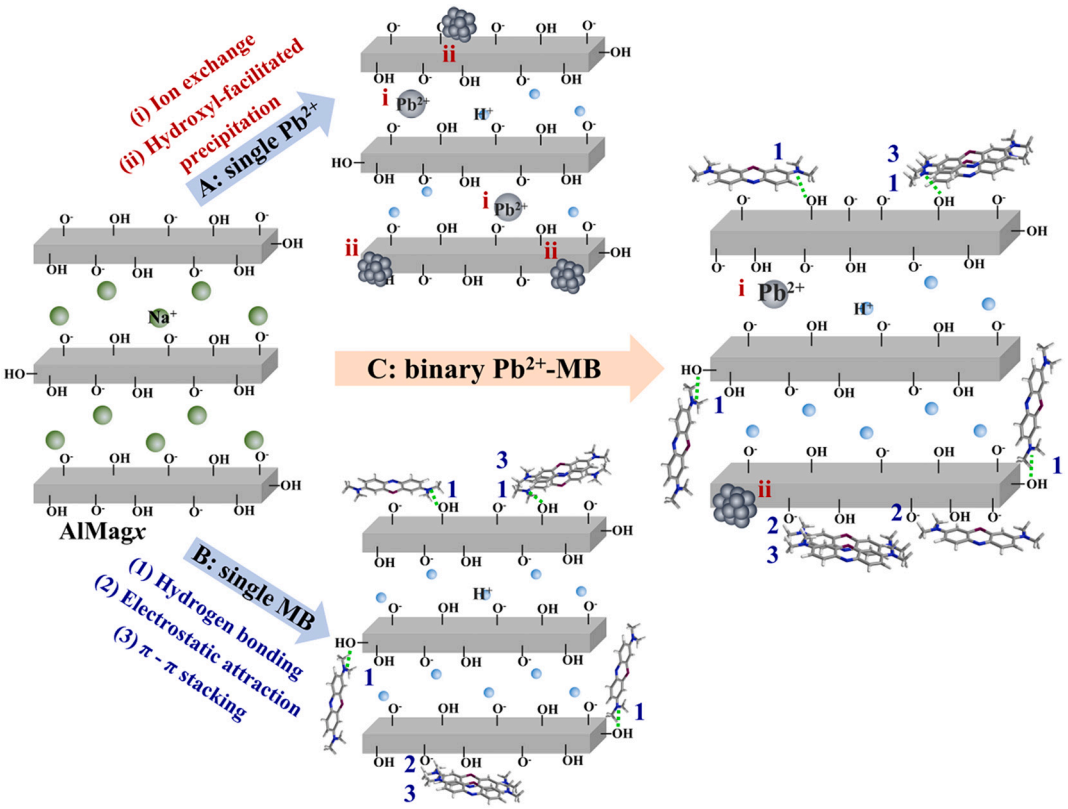

Fig. 8. Plausible adsorption mechanisms in the single Pb^{2+} (A), single MB (B), and binary Pb^{2+}–MB (C) solutions by AlMag*x* at pH 3.00.

CRediT authorship contribution statement

Qi Sun: Methodology, Investigation, Formal analysis, Writing – original draft. **Xingqiang Guo:** Software. **Bingchen Guo:** Data curation. **Qinyuan Tang:** Data curation. **Wenbin Yu:** Conceptualization, Writing – review & editing, Funding acquisition. **Quan Wan:** Resources, Supervision. **Yan An:** Resources, Supervision, Funding acquisition.

Declaration of Competing Interest

The authors declare that they have no known competing financial interests or personal relationships that could have appeared to influence the work reported in this paper.

Data availability

Data will be made available on request.

Acknowledgements

This work was supported by the Strategic Priority Research Program of Chinese Academy of Sciences (No. XDB 41000000), the National Natural Science Foundation of China (No. 41872046 and 41603065), and Guizhou Provincial Science and Technology Projects (No. [2019] 1318).

Appendix A. Supplementary data

Supplementary data to this article can be found online at https://doi.org/10.1016/j.clay.2022.106745.

References

Abdelhamid, H.N., 2020. Dye encapsulated hierarchical porous zeolitic imidazolate frameworks for carbon dioxide adsorption. J. Environ. Chem. Eng. 8, 104008 https://doi.org/10.1016/j.jece.2020.104008.

Abdellah, A.R., Abdelhamid, H.N., El-Adasy, A.-B.A.A.M., Atalla, A.A., Aly, K.I., 2020. One-pot synthesis of hierarchical porous covalent organic frameworks and two-dimensional nanomaterials for selective removal of anionic dyes. J. Environ. Chem. Eng. 8, 104054 https://doi.org/10.1016/j.jece.2020.104054.

Ajiboye, T.O., Oyewo, O.A., Onwudiwe, D.C., 2021. Simultaneous removal of organics and heavy metals from industrial wastewater: a review. Chemosphere 262, 128379. https://doi.org/10.1016/j.chemosphere.2020.128379.

Al-Ghouti, M.A., Da'ana, D.A., 2020. Guidelines for the use and interpretation of adsorption isotherm models: a review. J. Hazard. Mater. 393, 122383 https://doi.org/10.1016/j.jhazmat.2020.122383.

Al-Ghouti, M.A., Li, J., Salamh, Y., Al-Laqtah, N., Walker, G., Ahmad, M.N.M., 2010. Adsorption mechanisms of removing heavy metals and dyes from aqueous solution using date pits solid adsorbent. J. Hazard. Mater. 176, 510–520. https://doi.org/10.1016/j.jhazmat.2009.11.059.

Almeida, R.K.S., Paz, G.L., Báfero, G.B., Pastore, H.O., 2019. Properties of layered [Al]- and [V,Al]-magadiite catalysts as revealed by ethanol dehydration. Microporous Mesoporous Mater. 284, 1–9. https://doi.org/10.1016/j.micromeso.2019.04.002.

Bi, Y., Blanchard, J., Lambert, J.-F., Millot, Y., Casale, S., Zeng, S., Nie, H., Li, D., 2012. Role of the Al source in the synthesis of aluminum magadiite. Appl. Clay Sci. 57, 71–78. https://doi.org/10.1016/j.clay.2012.01.005.

Bi, J., Tao, Q., Huang, X., Wang, J., Wang, T., Hao, H., 2021. Simultaneous decontamination of multi-pollutants: a promising approach for water remediation. Chemosphere 284, 131270. https://doi.org/10.1016/j.chemosphere.2021.131270.

Chen, B., Zhao, H., Chen, S., Long, F., Huang, B., Yang, B., Pan, X., 2019. A magnetically recyclable chitosan composite adsorbent functionalized with EDTA for simultaneous capture of anionic dye and heavy metals in complex wastewater. Chem. Eng. J. 356, 69–80. https://doi.org/10.1016/j.cej.2018.08.222.

Ding, H., Chen, Y., Fu, T., Bai, P., Guo, X., 2018. Nanosheet-based magadiite: a controllable two-dimensional trap for selective capture of heavy metals. J. Mater. Chem. A 6, 13624–13632. https://doi.org/10.1039/C8TA04790A.

dos Santos, T.G., de Assis, G.C., da Silva, A.O.S., Meneghetti, S.M.P., 2022. Progress in development of magadiite to produce multifunctional lamellar materials. ACS Appl. Mater. Interfaces. https://doi.org/10.1021/acsami.1c15785.

Du, P., Xu, L., Ke, Z., Liu, J., Wang, T., Chen, S., Mei, M., Li, J., Zhu, S., 2022. A highly efficient biomass-based adsorbent fabricated by graft copolymerization: Kinetics, isotherms, mechanism and coadsorption investigations for cationic dye and heavy metal. J. Colloid Interface Sci. 616, 12–22. https://doi.org/10.1016/j.jcis.2022.02.048.

França, D.B., Torres, S.M., Filho, E.C.S., Fonseca, M.G., Jaber, M., 2019. Understanding the interactions between ranitidine and magadiite: influence of the interlayer cation. Chemosphere 222, 980–990. https://doi.org/10.1016/j.chemosphere.2019.01.154.

Gang, D., Uddin Ahmad, Z., Lian, Q., Yao, L., Zappi, M.E., 2021. A review of adsorptive remediation of environmental pollutants from aqueous phase by ordered mesoporous carbon. Chem. Eng. J. 403, 126286–126305. https://doi.org/10.1016/j.cej.2020.126286.

Ge, M., Cao, L., Du, M., Hu, G., Jahangir Alam, S.M., 2018. Competitive adsorption analyses of a pure magadiite and a new silylated magadiite on methylene blue and phenol from related aqueous solution. Mater. Chem. Phys. 217, 393–402. https://doi.org/10.1016/j.matchemphys.2018.02.052.

Georgouvelas, D., Abdelhamid, H.N., Li, J., Edlund, U., Mathew, A.P., 2021. All-cellulose functional membranes for water treatment: adsorption of metal ions and catalytic decolorization of dyes. Carbohydr. Polym. 264, 118044 https://doi.org/10.1016/j.carbpol.2021.118044.

Ghaedi, M., Mazaheri, H., Khodadoust, S., Hajati, S., Purkait, M.K., 2015. Application of central composite design for simultaneous removal of methylene blue and Pb^{2+} ions by walnut wood activated carbon. Spectrochim. Acta A 135, 479–490. https://doi.org/10.1016/j.saa.2014.06.138.

Hao, W., Flynn, S.L., Alessi, D.S., Konhauser, K.O., 2018. Change of the point of zero net proton charge (pHPZNPC) of clay minerals with ionic strength. Chem. Geol. 493, 458–467. https://doi.org/10.1016/j.chemgeo.2018.06.023.

Homhuan, N., Bureekaew, S., Ogawa, M., 2017. Efficient concentration of indium(III) from aqueous solution using layered silicates. Langmuir 33, 9558–9564. https://doi.org/10.1021/acs.langmuir.7b01575.

Ide, Y., Ochi, N., Ogawa, M., 2011. Effective and selective adsorption of Zn^{2+} from seawater on a layered silicate. Angew. Chem. Int. Edit. 123, 680–682. https://doi.org/10.1002/anie.201002322.

Kassem, A.A., Abdelhamid, H.N., Fouad, D.M., Ibrahim, S.A., 2020. Hydrogenation reduction of dyes using metal-organic framework-derived CuO@C. Microporous Mesoporous Mater. 305, 110340 https://doi.org/10.1016/j.micromeso.2020.110340.

Lim, W.T., Jang, J.H., Park, N.Y., Paek, S.M., Kim, W.C., Park, M., 2017. Spontaneous nanoparticle formation coupled with selective adsorption in magadiite. J. Mater. Chem. A 5, 4144–4149. https://doi.org/10.1039/C7TA00038C.

Liu, Q., Liu, Y., 2003. Distribution of Pb(II) species in aqueous solutions. J. Colloid Interface Sci. 268, 266–269. https://doi.org/10.1016/S0021-9797(03)00638-6.

Ma, L., Xi, Y., He, H., Ayoko, G.A., Zhu, R., Zhu, J., 2016. Efficiency of Fe–montmorillonite on the removal of Rhodamine B and hexavalent chromium from aqueous solution. Appl. Clay Sci. 120, 9–15. https://doi.org/10.1016/j.clay.2015.11.010.

Ma, Y.-X., Shao, W.-J., Sun, W., Kou, Y.-L., Li, X., Yang, H.-P., 2018. One-step fabrication of β-cyclodextrin modified magnetic graphene oxide nanohybrids for adsorption of Pb(II), Cu(II) and methylene blue in aqueous solutions. Appl. Surf. Sci. 459, 544–553. https://doi.org/10.1016/j.apsusc.2018.08.025.

Madduri, S., Elsayed, I., Hassan, E.B., 2020. Novel oxone treated hydrochar for the removal of Pb(II) and methylene blue (MB) dye from aqueous solutions. Chemosphere 260, 127683–127694. https://doi.org/10.1016/j.chemosphere.2020.127683.

Mokhtar, M., 2017. Application of synthetic layered sodium silicate magadiite nanosheets for environmental remediation of methylene blue dye in water. Materials 10, 760–772. https://doi.org/10.3390/ma10070760.

Mokhtar, A., Abdelkrim, S., Hachemaoui, M., Adjdir, M., Zahraoui, M., Boukoussa, B., 2020. Layered silicate magadiite and its composites for pollutants removal and antimicrobial properties: a review. Appl. Clay Sci. 198, 105823–105836. https://doi.org/10.1016/j.clay.2020.105823.

Moura, H.M., Bonk, F.A., Vinhas, R.C.G., Landers, R., Pastore, H.O., 2011. Aluminium-magadiite: from crystallization studies to a multifunctional material. Cryst. Eng. Comm. 13, 5428–5438. https://doi.org/10.1039/C1CE05213F.

Murakami, Y., Nanba, M., Tagashira, S., Sasaki, Y., 2006. Ion-exchange and structural properties of magadiite. Clay Sci. 12, 37–41. https://doi.org/10.11362/jcssjclayscience1960.12.Supplement2_37.

Ngulube, T., Gumbo, J.R., Masindi, V., Maity, A., 2017. An update on synthetic dyes adsorption onto clay based minerals: a state-of-art review. J. Environ. Manag. 191, 35–57. https://doi.org/10.1016/j.jenvman.2016.12.031.

Nimbalkar, M.N., Bhat, B.R., 2021. Simultaneous adsorption of methylene blue and heavy metals from water using Zr-MOF having free carboxylic group. J. Environ. Chem. Eng. 9, 106216 https://doi.org/10.1016/j.jece.2021.106216.

Oliveira, M.E.R., da Silva Filho, E.C., Filho, J.M., Ferreira, S.S., Oliveira, A.C., Campos, A. F., 2015. Catalytic performance of kenyaite and magadiite lamellar silicates for the production of α,β-unsaturated esters. Chem. Eng. J. 263, 257–267. https://doi.org/10.1016/j.cej.2014.11.016.

Ovchinnikov, O.V., Evtukhova, A.V., Kondratenko, T.S., Smirnov, M.S., Khokhlov, V.Y., Erina, O.V., 2016. Manifestation of intermolecular interactions in FTIR spectra of methylene blue molecules. Vib. Spectrosc. 86, 181–189. https://doi.org/10.1016/j.vibspec.2016.06.016.

Royer, B., Cardoso, N.F., Lima, E.C., Macedo, T.R., Airoldi, C., 2009. Sodic and acidic crystalline lamellar magadiite adsorbents for the removal of methylene blue from aqueous solutions: kinetic and equilibrium studies. Sep. Sci. Technol. 45, 129–141. https://doi.org/10.1080/01496390903256257.

Shannon, R.D., 1976. Revised effective ionic radii and systematic studies of interatomic distances in halides and chalcogenides. Acta Crystallogr. A 32, 751–767. https://doi.org/10.1107/S0567739476001551.

Sruamsiri, D., Sirinakorn, T., Ogawa, M., 2021. Efficient concentration of Pb^{2+} from water by reactions with layered alkali silicates, magadiite and octosilicate. Clay Clay Miner. 69, 416–424. https://doi.org/10.1007/s42860-021-00140-x.

Sun, Q., Zhang, C., Sun, H., Zhang, H., 2014. Aluminated derivatives of porous magadiite heterostructures for acid-catalyzed tert-butylation of catechol. Ind. Eng. Chem. Res. 53, 12224–12237. https://doi.org/10.1021/ie502266r.

Superti, G.B., Oliveira, E.C., Pastore, H.O., Bordo, A., Bisio, C., Marchese, L., 2007. Aluminum magadiite: an acid solid layered material. Chem. Mater. 19, 4300–4315. https://doi.org/10.1021/cm0707657.

Thommes, M., Kaneko, K., Neimark, A.V., Olivier, J.P., Rodriguez-Reinoso, F., Rouquerol, J., Sing, K.S.W., 2015. Physisorption of gases, with special reference to the evaluation of surface area and pore size distribution (IUPAC Technical Report). Pure Appl. Chem. 87, 1051–1069. https://doi.org/10.1515/pac-2014-1117.

Tombácz, E., Szekeres, M., 2004. Colloidal behavior of aqueous montmorillonite suspensions: the specific role of pH in the presence of indifferent electrolytes. Appl. Clay Sci. 27, 75–94. https://doi.org/10.1016/j.clay.2004.01.001.

Uddin, M.K., 2017. A review on the adsorption of heavy metals by clay minerals, with special focus on the past decade. Chem. Eng. J. 308, 438–462. https://doi.org/10.1016/j.cej.2016.09.029.

Zebib, B., Lambert, J.-F., Blanchard, J., Breysse, M., 2006. LRS-1: a new delaminated phyllosilicate material with high acidity. Chem. Mater. 18, 34–40. https://doi.org/10.1021/cm050643j.

Zhao, F., Repo, E., Yin, D., Meng, Y., Jafari, S., Sillanpää, M., 2015. EDTA-cross-linked β-cyclodextrin: an environmentally friendly bifunctional adsorbent for simultaneous adsorption of metals and cationic dyes. Environ. Sci. Technol. 49, 10570–10580. https://doi.org/10.1021/acs.est.5b02227.